MSDE

Molecular Systems Design & Engineering

ROYAL SOCIETY
OF CHEMISTRY
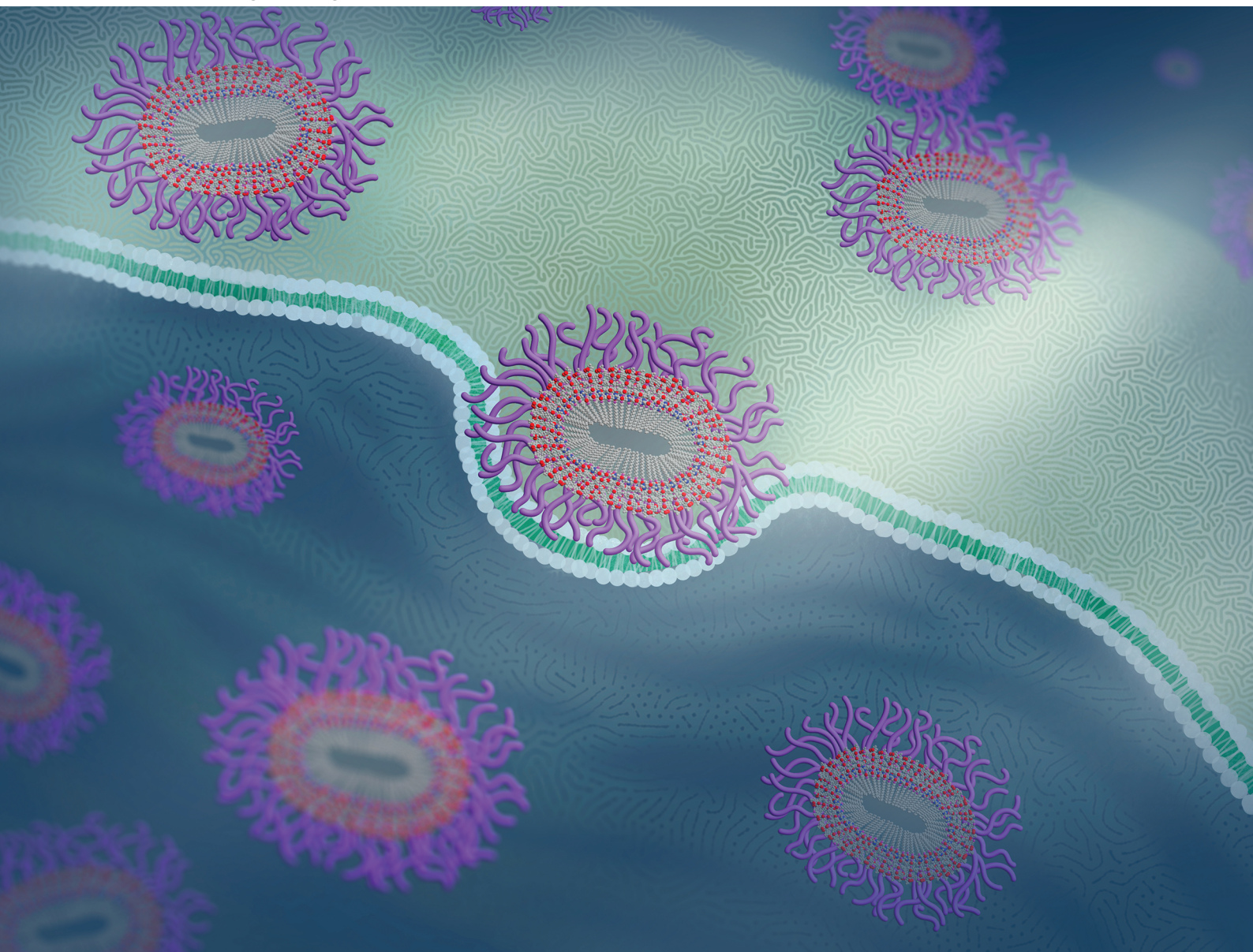
PAPER
Bret D. Ulery *et al.*
Vasoactive intestinal peptide amphiphile micelle material
properties influence their cell association and internalization

IChemE ADVANCING CHEMICAL ENGINEERING WORLDWIDE

Vasoactive intestinal peptide amphiphile micelle material properties influence their cell association and internalization

Xiaofei Wang,[a] Agustin T. Barcellona,[a] Fateme Nowruzi,[a] Kambrie M. Brandt,[a] Megan C. Schulte,[a] Luke E. Kruse,[a] Eric Dong,[a] Adam G. Schrum,[abcd] Esma S. Yolcu[bde] and Bret D. Ulery [iD] *[adf]

Vasoactive intestinal peptide (VIP) is a promising anti-inflammatory peptide therapeutic that is known to induce biological effects by interacting with its cognate receptor (*i.e.*, VPAC) on the surface of antigen presenting cells (APCs). Little is known about how VPAC targeting affects APC behavior for VIP-based drug delivery systems like nano- and microparticles. This is further influenced by the fact that particulate material properties including chemistry, shape, and size are all known to influence APC behavior. In this study, peptide amphiphile micelles (PAMs) were employed as a modifiable platform to study the impact VPAC targeting and physical particle properties have on their association with macrophages. VIP amphiphile micelles (VIPAMs) and their scrambled peptide amphiphile micelle analogs (SVIPAMs) were fabricated from various chemistries yielding particle batches that were comprised of spheres (10–20 nm in diameter) and/ or cylinders of varying lengths (*i.e.*, 20–9000 nm). Micelle surface attachment to and internalization by macrophages were observed using confocal microscopy and their association was characterized by flow cytometry. The enclosed work provides strong evidence that macrophages rapidly bind VPAC specific micelles, and that micelle shape, size, and receptor-specificity all influence macrophage association and internalization. Specifically, a mixture of spherical and short cylindrical VIPAMs were able to achieve the greatest cell association which may correlate to their capacity to fully bind the VPAC receptors available on the surface of macrophages. These results provide the foundation of how nano- and microparticle physical properties and targeting capacity combine to influence their capacity to associate with APCs.

Design, System, Application

Effective delivery of peptides and peptide-based therapeutics is limited by several obstacles including rapid enzymatic degradation, structural disorganization, and low molecular selectivity. In this work, we utilized previously established design criteria to construct peptide amphiphiles (PAs) which have the capacity to self-assemble into stable, nanostructured peptide amphiphile micelles (PAMs) in water. PAMs serve as a promising delivery platform for enhancing therapeutic payload and improving cellular interactions, though micelle bioactivity and architecture are significantly influenced by the molecular composition of the PA and its components. Here, we attached single- or double-lipid moieties and zwitterion-like blocks with different sequences onto the respective N- and C-termini of the therapeutic peptide yielding PAMs with various shapes and surface properties. Assessment of critical micelle concentration, surface charge, size, and secondary structure was carried out for each micelle formulation, and cell association was measured for the purpose of determining which PAM architecture most efficiently transported the therapeutic payload. Double-lipid, balanced zwitterion-like block PAMs were found to have the greatest level of cellular interactions, demonstrating their potential for controlled, targeted peptide delivery. Future directions will focus on leveraging the tunability of PAMs to co-deliver highly specific targeting aptamers, molecular adjuvants, and fluorescent trackers for enhanced therapeutic and diagnostic functions.

[a] *Department of Chemical and Biomedical Engineering, University of Missouri, Columbia, MO 65211, USA. E-mail: uleryb@missouri.edu*

[b] *Department of Molecular Microbiology and Immunology, University of Missouri, Columbia, MO 65211, USA*

[c] *Department of Surgery, University of Missouri, Columbia, MO 65211, USA*

[d] *NextGen Precision Health Institute, University of Missouri, Columbia, MO 65211, USA*

[e] *Department of Pediatrics, University of Missouri, Columbia, MO 65211, USA*

[f] *Materials Science and Engineering Institute, University of Missouri, Columbia, MO 65211, USA*

Introduction

Vasoactive intestinal peptide (VIP) is an endogenous neuropeptide that has emerged as a promising immunomodulatory candidate for treating a wide variety of inflammatory conditions.[1] VIP adeptly mitigates proinflammatory cytokine expression, promotes anti-inflammatory activity, and modulates immune cell processes, contributing to a balanced immune homeostasis.[2,3] Despite

its safety and efficacy, the clinical development of VIP as an immunotherapeutic agent faces several challenges including possessing a very short half-life and undesirable off-target effects.[4] To overcome these limitations, researchers have begun engineering VIP using various approaches to improve its pharmaceutical properties while maintaining or enhancing its immunomodulatory activity.[5] In the context of peptide therapeutics, lipidation has been found to enhance peptide delivery and bioactivity[6,7] making this a promising approach for VIP delivery. Despite the successes of lipid–peptide drug conjugates, further investigation is needed into the role that structure and other material properties have on their biological effects.

Peptide amphiphiles (PAs) are lipid-modified peptides that self-assemble into nanostructured peptide amphiphile micelles (PAMs) in water. PAMs offer several advantages that overcome the limitations associated with free peptide administration; they can prevent peptidyl diffusion,[8] increase local peptide concentration,[9] enhance intracellular peptide delivery,[10] and improve peptide bioactivity.[11] The effects of PAMs on the immune system depend on different factors, including, but not limited to, the shape and size of micelles.[12,13] Specifically, these factors can affect micelle–cell association and internalization, contributing to the activation of antigen presenting cells (APCs) to an inflammatory state.[14,15] Therefore, the investigation of macrophage association with and uptake of micelles of different shapes and sizes is crucial to understanding how they affect the immune system. Moreover, most studies have focused on the cell processing of solid particles (i.e., polymeric,[16,17] silica,[18,19] and metallic[20,21]) which may behave differently than supramolecular particles like PAMs.[22] Importantly, few studies analyzing VIP amphiphile micelle (VIPAM) structure and shape as well as their effects on the immune system and cell interactions have been undertaken. Recently, our research group synthesized a small library of VIPAMs containing different N-terminal palmitoyl and dipalmitoyllysine moieties and zwitterion-like lysine–glutamic acid peptide segments which includes PalmK-$(EK)_4$-VIP, PalmK-VIP-$(KE)_4$, $Palm_2K$-$(EK)_4$-VIP, and $Palm_2K$-VIP-$(KE)_4$. Morphological assessments demonstrated that the zwitterion-like block location within the PAs greatly impacted the assembly, structure, and charge of VIPAMs which influenced their stability, cell interactions, and bioactivity.[23] Based on this work, external zwitterion-like block-VIPAs were selected for further study due to their optimized shape, size, charge, and durable anti-inflammatory effects.

This study further investigates the intricate interplay between the physical properties of VIPAMs and their cellular interactions with macrophages. Here, we synthesized and characterized a new VIPA library which includes PalmK-VIP-$(KE)_4$, $Palm_2K$-VIP-$(KE)_4$, $Palm_2K$-VIP-$(KE)_2K_4$ and $Palm_2K$-VIP-$(KE)_2E_4$. The modification of the $(KE)_4$ block was specifically targeted as this can allow for modification of micellar shape, an aspect of significant importance for cell–nanoparticle interactions.[10,11,16] Scrambled analogs of these products (i.e.,

$PalmK$-^SVIP-$(KE)_4$, $Palm_2K$-^SVIP-$(KE)_4$, $Palm_2K$-^SVIP-$(KE)_2K_4$, and $Palm_2K$-^SVIP-$(KE)_2E_4$) were also synthesized since these allow for the probing of the role receptor-specific interactions have on VIPAM bioactivity.

The strategic design of PAMs with external zwitterion-like lysine–glutamic acid sequences and dipalmitoyllysine additions was employed to help optimize VIP delivery and bioactivity. Specifically, structurally unique VIPAMs were formed with shapes ranging from small spheres to long cylinders. VIPAM shapes were controlled by altering both the ratio of lysine to glutamic acid within the $(KE)_x$ sequences as well as the number of hydrocarbon tails in the lipid moiety. Interestingly, micelle shape and size directly influenced cellular association and internalization. This effect demonstrated the clear benefit of utilizing PAMs to effectively deliver VIP to target cells for immunomodulation. Additionally, these findings open new possibilities for developing advanced immunotherapies leveraging the unique functional capacity of PAMs.
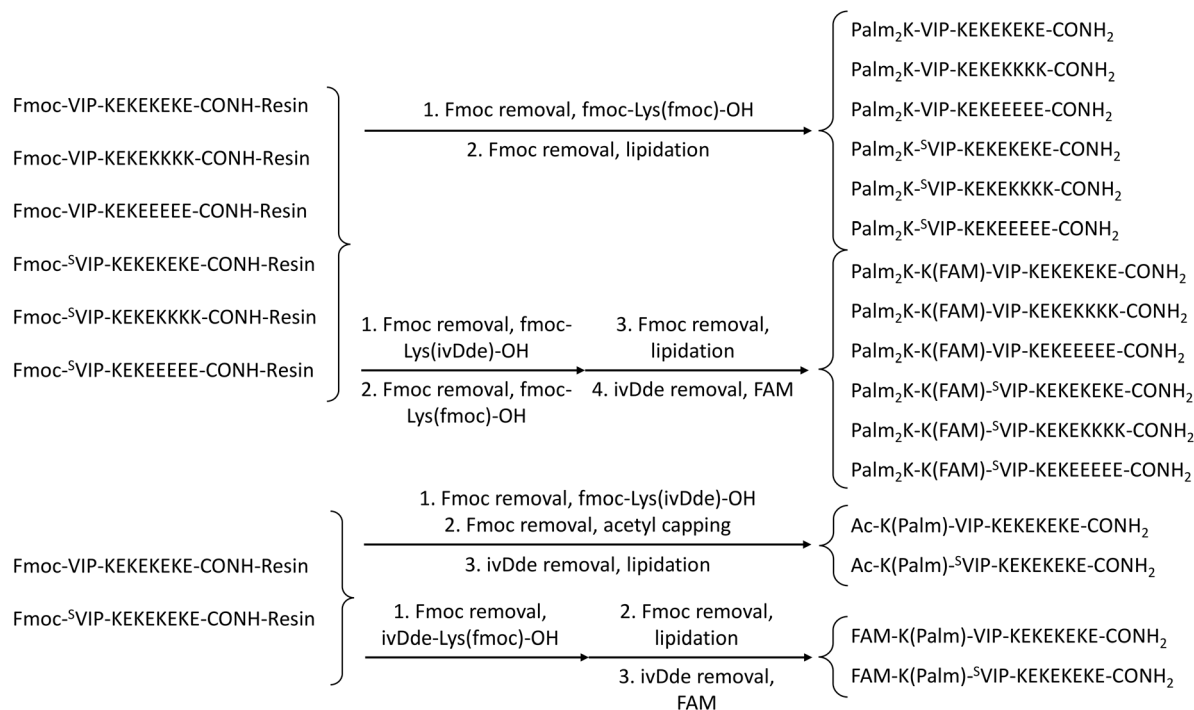
Materials and methods

Vasoactive intestinal peptide (VIP, Ac-HSDAVFTDNYTRLRKQMAVKKYLNSILN-$CONH_2$), scrambled VIP (^SVIP, Ac-NSDLIATDSYTRMRKQVLANKKFHYLVN-$CONH_2$), Fmoc-VIP-KEKEKEKE-CONH-Resin, Fmoc-^SVIP-KEKEKEKE-CONH-Resin, Fmoc-VIP-KEKEKKKK-CONH-Resin, Fmoc-^SVIP-KEKEKKKK-CONH-Resin, Fmoc-VIP-KEKEEEEE-CONH-Resin, and Fmoc-^SVIP-KEKEEEEE-CONH-Resin were purchased from Synpeptide Co., Ltd, China. Fmoc-Lys(Fmoc)-OH, Fmoc-Lys(ivDde)-OH, and ivDde-Lys(Fmoc)-OH were acquired from Novabiochem. AK Scientific, Inc. and AnaSpec, Inc. were the suppliers used for 2-(1H-benzotriazol-1-yl)-1,1,3,3-tetramethyluronium hexafluorophosphate (HBTU) and 1-hydroxybenzotriazole hydrate (HOBt hydrate), respectively. Palmitic acid (Palm) and 5(6)-carboxyfluorescein (FAM) were acquired from Acros Organics. Piperidine, triisopropylsilane (TIS), N,N-diisopropylethylamine (DIEA) were purchased from Chem-Impex International, Inc. Dimethylformamide (DMF), 1-methyl-2-pyrrolidinone (NMP), acetic anhydride (Ac_2O), hydrazine monohydrate, thioanisole (TA), trifluoroacetic acid (TFA), phenol, ethanedithiol (EDT), and diethyl ether were bought from Millipore Sigma. A glass peptide reaction vessel was obtained from Chemglass Life Sciences. Fetal bovine serum (FBS) was sourced from Sigma Aldrich, located in St. Louis, MO. Penicillin/streptomycin solution was purchased from ThermoFisher, based in Waltham, MA. Lipopolysaccharide (LPS) was obtained from Santa Cruz Biotechnology, Inc., Dallas, TX. The molecule 1,6-diphenyl-1,3,5-hexatriene (DPH) was acquired from Sigma Aldrich, St. Louis, MO.

Solid phase peptide synthesis (SPPS) and lipidation

The library of VIP and ^SVIP products were synthesized on a resin support employing standard Fmoc solid phase peptide synthesis (SPPS) using our previously reported method.[23] The general approach for the synthesis of the PA formulations is

This journal is © The Royal Society of Chemistry and IChemE 2025

Mol. Syst. Des. Eng., 2025, 10, 534–548 | 535

Fmoc-VIP-KEKEKEKE-CONH-Resin
Fmoc-VIP-KEKEKKKK-CONH-Resin
Fmoc-VIP-KEKEEEEE-CONH-Resin
Fmoc-^{S}VIP-KEKEKEKE-CONH-Resin
Fmoc-^{S}VIP-KEKEKKKK-CONH-Resin
Fmoc-^{S}VIP-KEKEEEEE-CONH-Resin

1. Fmoc removal, fmoc-Lys(fmoc)-OH
2. Fmoc removal, lipidation

→

Palm$_2$K-VIP-KEKEKEKE-CONH$_2$
Palm$_2$K-VIP-KEKEKKKK-CONH$_2$
Palm$_2$K-VIP-KEKEEEEE-CONH$_2$
Palm$_2$K-^{S}VIP-KEKEKEKE-CONH$_2$
Palm$_2$K-^{S}VIP-KEKEKKKK-CONH$_2$
Palm$_2$K-^{S}VIP-KEKEEEEE-CONH$_2$

1. Fmoc removal, fmoc-Lys(ivDde)-OH
2. Fmoc removal, fmoc-Lys(fmoc)-OH
3. Fmoc removal, lipidation
4. ivDde removal, FAM

→

Palm$_2$K-K(FAM)-VIP-KEKEKEKE-CONH$_2$
Palm$_2$K-K(FAM)-VIP-KEKEKKKK-CONH$_2$
Palm$_2$K-K(FAM)-VIP-KEKEEEEE-CONH$_2$
Palm$_2$K-K(FAM)-^{S}VIP-KEKEKEKE-CONH$_2$
Palm$_2$K-K(FAM)-^{S}VIP-KEKEKKKK-CONH$_2$
Palm$_2$K-K(FAM)-^{S}VIP-KEKEEEEE-CONH$_2$

Fmoc-VIP-KEKEKEKE-CONH-Resin
Fmoc-^{S}VIP-KEKEKEKE-CONH-Resin

1. Fmoc removal, fmoc-Lys(ivDde)-OH
2. Fmoc removal, acetyl capping
3. ivDde removal, lipidation

→

Ac-K(Palm)-VIP-KEKEKEKE-CONH$_2$
Ac-K(Palm)-^{S}VIP-KEKEKEKE-CONH$_2$

1. Fmoc removal, ivDde-Lys(fmoc)-OH
2. Fmoc removal, lipidation
3. ivDde removal, FAM

→

FAM-K(Palm)-VIP-KEKEKEKE-CONH$_2$
FAM-K(Palm)-^{S}VIP-KEKEKEKE-CONH$_2$

Scheme 1 Fluorophore labeled and non-fluorophore labeled VIP amphiphiles and ^{S}VIP amphiphiles synthesis approaches.

outlined in Scheme 1. The dry resin was rinsed with NMP for 2 hours under a nitrogen atmosphere with bubbling to provide mixing. Between each step, the resin was pre-washed three times with the solvent for the next coupling or deprotection reaction. Fmoc deprotection was achieved by treatment with 25% piperidine in DMF (2 × 30 min). The ivDde protecting group was removed using 2% hydrazine monohydrate in DMF (6 × 20 min). For amino acid or lipid conjugation, Fmoc-Lys(ivDde)-OH, ivDde-Lys(Fmoc)-OH, Fmoc-Lys(Fmoc)-OH, or palmitic acid (1 equiv.) were pre-activated with HBTU (4.2 equiv.), HOBt (5 equiv.), and DIEA (10 equiv.) in NMP for 10 min. The activated species were then coupled to the N-terminus of the resin-bound peptide over three 90 min coupling cycles. For fluorescent labeling, FAM (1 equiv.) was pre-activated similarly using HBTU/HOBt/DIEA and coupled to the N-terminus over three overnight cycles. Remaining unreacted N-termini were capped by treatment with 5% acetic anhydride and 7% DIEA in NMP for 15 min.

After modifications, the resin was washed with methanol (3×), transferred to a 15 mL centrifuge tube as a methanol slurry, and dried under high vacuum. Peptide cleavage from the resin and global deprotection of side chains was achieved by a 2 h treatment with a cleavage cocktail of TFA/thioanisole/triisopropylsilane/water/phenol/ethanedithiol (87.5 : 2.5 : 2.5 : 2.5 : 2.5 : 2.5). Cleaved peptides were precipitated in diethyl ether and then centrifuged. The solid was collected, resuspended in fresh diethyl ether by vortexing (3×) to wash the solids, and finally dissolved in minimal deionized water for lyophilization to yield the purified product as a powder. All crude VIP and VIP amphiphiles (VIPAs) as well as their scrambled analogues were analyzed by an analytical high-pressure liquid chromatograph (HPLC, Beckman Coulter) and purified by preparative mass-spectrometry fraction-controlled HPLC (HPLC-MS) on a C4 column (Milford, MA).

Critical micelle concentration (CMC)

A critical micelle concentration (CMC) assay was performed to determine the concentration at which different VIPAs and ^{S}VIPAs form micelles in. In this study, DPH was employed as a fluorophore to determine the CMC. DPH can exhibit weak fluorescence in aqueous environments, but becomes strongly fluorescent when incorporated within a hydrophobic domain. PAs were serially diluted (31.6 μM to 0 μM) in 1 μM DPH in phosphate buffered saline (PBS) and allowed to incubate for at least 1 hour. Sample fluorescence was measured by a Cytation 5 fluorospectrophotometer (BioTek Instruments, Inc., Winooski, VT) at ex: 350 nm, em: 428 nm. The jerk point between stable low fluorescence and the beginning of a rapid increase in fluorescence was considered the CMC for the sample.

Micelle morphology characterization

PAM morphology was characterized by negative-stain transmission electron microscopy (TEM) using a previously established method.[23] Micelle solution (5 μM) was added to a carbon support TEM grid (200 mesh, Electron Microscopy Sciences, Hatfield, PA). After 5 minutes of incubation, the solution was removed and immediately followed by the addition of 5 μL of NanoW (Nanoprobes, Inc, Yaphank, NY). After 3 minutes of incubation, the solution was removed and grids were left to dry followed by imaging with a JEOL JEM-

536 | *Mol. Syst. Des. Eng.*, 2025, **10**, 534–548

This journal is © The Royal Society of Chemistry and IChemE 2025

1400 TEM at 120 kV. Images of at least three different spots on each grid were taken and analyzed.

Size and surface charge measurement

The size and surface charge of micelles were determined by measuring dynamic light scattering and zeta potential, respectively, using a Malvern zetasizer (Malvern, UK). For dynamic light scattering, PAM product solutions (200 μL) were prepared at a concentration of 5 μM in 2% PBS in deionized, distilled water (ddH$_2$O) and measured using the backscattering method. For zeta potential measurement, solutions (750 μL) were prepared to a concentration of 10 μM in 2% PBS in ddH$_2$O and assessed by the Smoluchowski method.

Secondary structure measurement

Micelle secondary structure was assessed by circular dichroism (CD) using a Chirascan V100 CD spectrometer from Applied PhotoPhysics (Leatherhead, UK). Micelle solutions (40 μM) were prepared in PBS and loaded into a 0.5 mm cuvette and measured spectrophotometrically from 200 nm to 250 nm with an interval of 1 nm. The data were fit using a linear combination of polylysine and polyglutamine structures to calculate approximate α-helical, β-sheet, and random coil content.

Cell assessment

Immunomodulatory experiments were conducted with murine RAW 264.7 (macrophage-like cells – Mφs) using an established protocol.[23] Complete Dulbecco's modified Eagle medium (DMEM) was made by supplementing DMEM with 1% penicillin/streptomycin (ThermoFisher, Waltham, MA), and 10% FBS (FBS, Sigma Aldrich, St. Louis, MO). Mφs were cultured in 100 mm diameter, non-treated Petri-dishes in complete DMEM at 37 °C and 5% CO$_2$. The cells were seeded in non-tissue culture treated 24-well plates at 50 000 cells per well. After overnight incubation in complete DMEM, cells were stimulated with 0.1 μg mL^{-1} of LPS (Santa Cruz Biotechnology, Inc., Dallas, TX) along with varying concentrations of VIP, VIPAs, ^{S}VIP, or ^{S}VIPAs. All peptides were non-fluorophore labeled whereas micelle products possessed small amounts of fluorophore labeled components (i.e., 1 : 19 FAM-PA : non-FAM-PA). Cells given media alone without the LPS stimulus were studied as a negative control. After 1 or 6 hours of incubation, supernatant solutions were collected for assessment of secreted tumor necrosis factor-α (TNF-α) content using an enzyme-linked immune sorbent assay (ELISA) kit (Biolegend, San Diego, CA). Cells were washed with PBS to delaminate them from the bottom of the non-tissue culture treated 24-well plates after which a second wash with PBS was performed to ensure the collection of all cells. To analyze viability, the collected cells were stained with the Live-or-Dye 594/614 Fixable Viability Staining Kit™ (Biotium, Fremont, CA) and then analyzed by a flow cytometer (BD LSRFortessa X20) equipped with FACSDiva 8.0 Software to detect the fluorescence intensity of each cell.

FlowJo was utilized to gate the cells and analyze the fluorescence signals.

For microscopy studies, cover slips were added to the non-tissue culture treated 24-well plates before 0.05 million cells were placed in each well. After overnight incubation, cells were treated with 0.1 μg mL^{-1} of LPS containing the same VIPAs or ^{S}VIPAs possessing small amounts of fluorophore labeled components (i.e., 1 : 19 FAM-PA : non-FAM-PA) as was used for the previous studies. After 1 hour or 6 hours of incubation, cells bound to coverslips were washed with Hank's balanced salt solution (HBSS) and stained with 5 μg mL^{-1} wheat germ agglutinin (WGA) for 10 minutes at 37 °C and 5% CO$_2$. Cells were then washed twice with PBS to remove any non-associated stain. Cells were fixed through exposure to 4% paraformaldehyde (PFA) for 15 minutes. A total of three PBS washes were used to get rid of any excess PFA and then cells were subjected to 1% Triton X-100 for 15 minutes to help permeabilize the fixed cell membrane. After washing the cells three times with PBS, they were preincubated with 1% bovine serum albumin (BSA) in PBS for 30 minutes to prevent non-specific binding of the 4,6′-diamidino-2-phenylindole (DAPI) stain used to identify the cell nucleus. DAPI-containing mounting solution was then used to adhere the cover slip to glass slides that were then analyzed for their fluorescence using a Leica TCS SP8 STED and MP confocal microscope. Leica LAS X 3D Analysis software was employed to analyze, compile, and present the fluorescent data from the three channels used (i.e., 420–480 nm, 500–550 nm, and 670–730 nm).

Statistical analysis

The analysis of group comparisons was conducted using JMP software from SAS Institute (Cary, NC). This involved performing an analysis of variance (ANOVA) assessment followed by Tukey's honest significant differences (HSD) test to identify pairwise statistically significant differences ($p < 0.05$). In visual representations, groups with distinct letters or marked by a "*" signify statistically significant differences in means, whereas groups with the same letter or no symbol suggest statistically insignificant differences. All experiments were conducted with a group size of four replicates to ensure reproducibility and reliability.

Results and discussion

Bioactive concentration determination, chemical structure, and physical properties of VIPAs and ^{S}VIPAs

In order to investigate the impact micelle structural changes have on Mφ association, the previously studied double lipid, external zwitterion-like peptide block VIPA formulation (i.e., Palm$_2$K-VIP-(KE)$_4$) was selected as a starting PA from which to design new products as it displayed interesting concentration-, shape-, and size-dependent TNF-α expression modulation behavior, especially when compared to its long cylindrical, single lipid analog (i.e., PalmK-VIP-(KE)$_4$).[23] An initial dose effect study was completed to determine the

optimal concentration for these VIPAMs and their unlipidated, unmicellized peptide controls. Minimal impact on cell viability (Fig. 1a) in conjunction with TNF-alpha reduction (Fig. 1b) was observed at 5 μM. Structurally distinct VIPAM formulations homologous to $Palm_2K$-VIP-$(KE)_4$ were then generated in order to study the influence micelle architecture has on Mφ association and uptake. Incorporation of several lysine residues has been shown to reduce micelle size[24] likely due to corona-based charge repulsion increasing micelle surface curvature yielding spherical micelles in accordance with Israelachivili's surfactant theory.[25] Specifically, this theory defines a critical packing parameter (CPP) of surfactant molecules like PAs as:

$$CPP = \frac{v}{a_o \times l_c}$$

where v represents the hydrocarbon core volume, a_o is the effective head group area, and l_c is the hydrocarbon chain length. Based on this concept, the VIPAM hydrophilic peptide block (i.e., $(KE)_4$) was modified to contain short charge repulsive regions at the peptide C-terminus. Specifically, the last four amino acids were made all positive (i.e., $-(KE)_2K_4$ – zwit-cat) or all negative (i.e., $-(KE)_2E_4$ – zwit-an) yielding PAs with sequences of $Palm_2K$-VIP-$(KE)_2K_4$ and $Palm_2K$-VIP-$(KE)_2E_4$ (Table 1).

In addition to the four VIPAM formulations, a scrambled VIP peptide (^{S}VIP) was synthesized and utilized to generate ^{S}-VIPAM analogs to explore the influence peptide specificity has on micelle association and internalization by cells. In order to generate a non-functional, biocompatible scrambled peptide control, an algorithm employing a Boltzmann Factor scoring function was first utilized to rearrange the native VIP peptide sequence.[26] Amino acids known to participate in receptor binding were rearranged with residues possessing similar hydropathy, while minimal modifications were performed for amino acids which contribute to overall VIP structural integrity.[27] The final sequence of ^{S}VIP peptide and how it compares to VIP can be found in Table 1. Cytotoxicity and bioactivity studies were performed with ^{S}VIP and VIP at 5 μM using LPS-treated Mφs along with LPS-treated cells with no stimulus and non-LPS treated cells (Fig. 2). The viability of ^{S}VIP-treated cells remained high, though their secreted TNF-α concentration was slightly higher than those exposed to LPS alone possibly due to the formation of amorphous aggregates at 5 μM (Fig. 3) which might be responsible for inducing mild, non-specific inflammation in Mφs.[28,29] In contrast, VIP lacks any particle structure when observed by TEM (data not shown). Upon the identification of this appropriate ^{S}VIP peptide, a series of amphiphiles with the same chemical composition as the aforementioned VIPAs were produced by replacing the VIP block with ^{S}VIP yielding
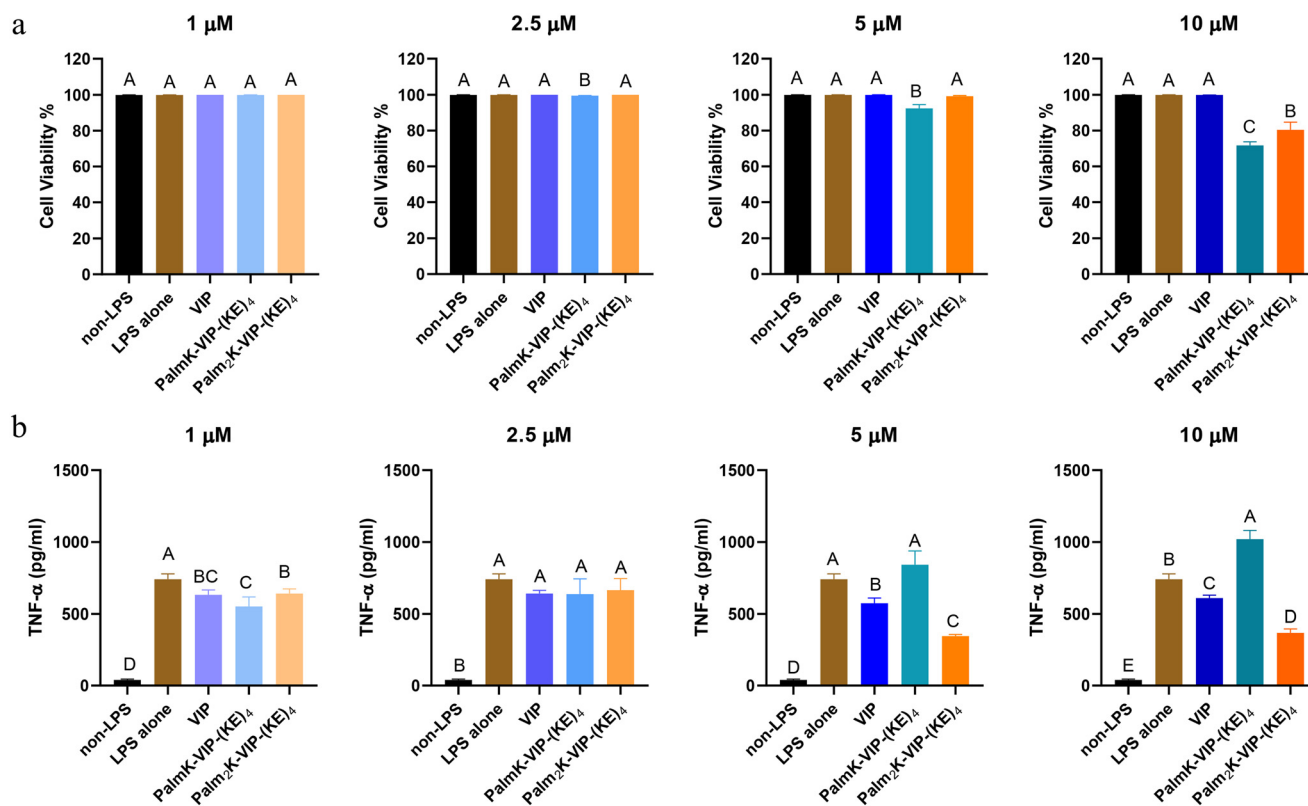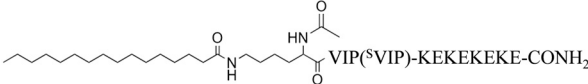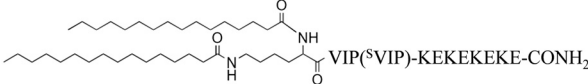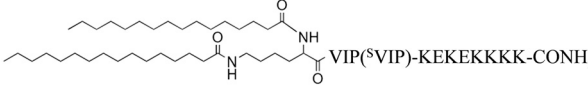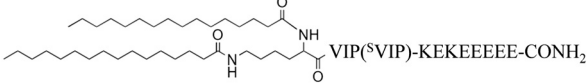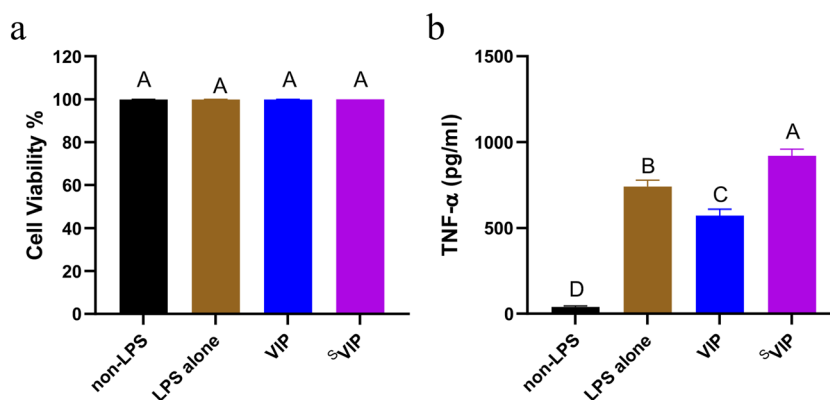

Fig. 1 Effect of VIPAM exposure on LPS–activated Mφ cell health (a) and TNF-α secretion (b). For all concentrations, LPS treatments were carried out for 6 hours (n = 4). In each graph, groups possessing the same letter have no statistically significant difference (p > 0.05).

Table 1 Sequences of VIP and ^{S}VIP and chemical structures of VIPAs and ^{S}VIPAs

VIP, ^{S}VIP and VIP (^{S}VIP) Amphiphiles	Abbreviations
Ac-HSDAVFTDNYTRLRKQMAVKKYLNSILN-CONH$_2$	VIP
Ac-NSDLIATDSYTRMRKQVLANKKFHYLVN-CONH$_2$	^{S}VIP
	PalmK-VIP-(KE)$_4$ or PalmK-^{S}VIP-(KE)$_4$
VIP(^{S}VIP)-KEKEKEKE-CONH$_2$	
	Palm$_2$K-VIP-(KE)$_4$ or Palm$_2$K-^{S}VIP-(KE)$_4$
VIP(^{S}VIP)-KEKEKEKE-CONH$_2$	
	Palm$_2$K-VIP-(KE)$_2$K$_4$ or Palm$_2$K-^{S}VIP-(KE)$_2$K$_4$
VIP(^{S}VIP)-KEKEKKKK-CONH$_2$	
	Palm$_2$K-VIP-(KE)$_2$E$_4$ or Palm$_2$K-^{S}VIP-(KE)$_2$E$_4$
VIP(^{S}VIP)-KEKEEEEE-CONH$_2$	

Fig. 2 Influence of 6 hour 5 μM ^{S}VIP exposure on LPS–activated Mφ cell health (a) and TNF-α secretion (b). In each graph (n = 4), groups possessing the same letter have no statistically significant difference ($p > 0.05$).

non-specific, scrambled micelles (^{S}VIPAMs) for further investigation (Table 1).

Once all VIPA and ^{S}VIPA formulations were synthesized (*i.e.*, PalmK-VIP-(KE)$_4$, Palm$_2$K-VIP-(KE)$_4$, Palm$_2$K-VIP-(KE)$_2$K$_4$ and Palm$_2$K-VIP-(KE)$_2$E$_4$, and ^{S}VIP analogs), CMCs were
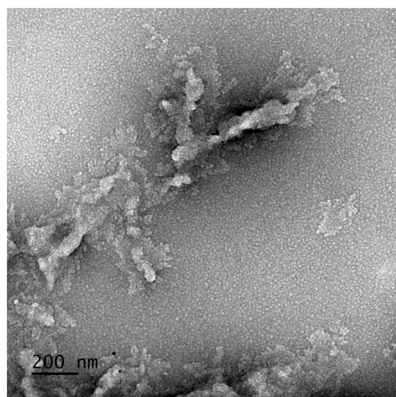
Fig. 3 Amorphous aggregates formed for ^{S}VIP at 5 μM. The micrograph was taken at a magnification of 12 000× with the scale bar representing 200 nm.

obtained to determine the minimal PA concentrations necessary for micelle formation as well as to observe the relationship between PA chemical structure and micellization (Fig. 4). All four VIPAs possessed relatively low CMCs with two formulations (*i.e.*, Palm$_2$K-VIP-(KE)$_4$ and Palm$_2$K-VIP-(KE)$_2$E$_4$) exhibiting a second CMC possibly indicating a secondary micelle structure transition. When looking at the initial CMC values for each formulation, single lipid VIPAs (*i.e.*, PalmK-VIP-(KE)$_4$) had the highest concentration (Fig. 4a – 0.333 μM). Interestingly, Palm$_2$K-VIP-(KE)$_4$ had a lower CMC (Fig. 4b – 0.0872 μM) than both single lipid VIPAs and double lipid VIPAs possessing uneven ratios of either lysines or glutamic acids (*i.e.*, Fig. 4c – Palm$_2$K-VIP-(KE)$_2$K$_4$ – 0.304 μM and Fig. 4d – Palm$_2$K-VIP-(KE)$_2$E$_4$ – 0.182 μM). We have previously noted the lipid number effect as being likely due to lipid–peptide hydrophobicity differences influencing micellization[23] and now the new charge block effect could potentially arise from charge repulsion between the hydrophilic head groups.[30] The CMCs of the four ^{S}VIPA analogs were determined to better understand the influence bioactive peptide chemical structure has on micelle formation and architecture (Fig. 4e–h). The physical
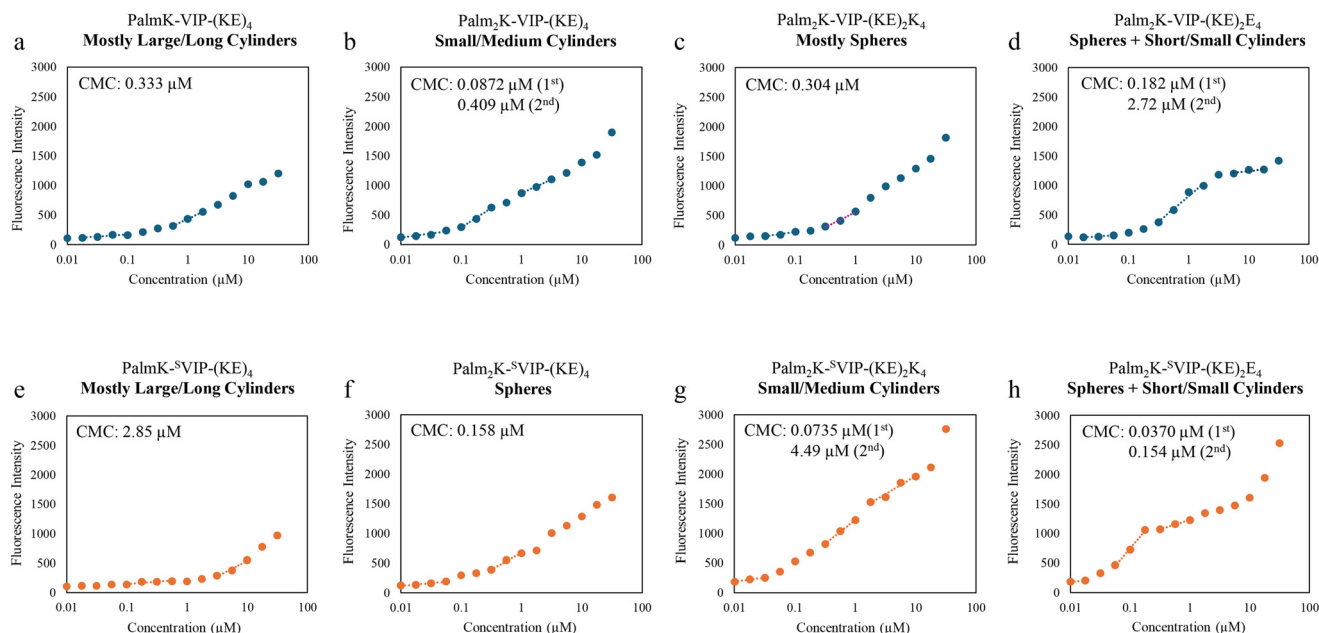
This journal is © The Royal Society of Chemistry and IChemE 2025

Mol. Syst. Des. Eng., 2025, **10**, 534–548 | **539**

Fig. 4 Critical micelle concentration (CMC) and all VIPAM formulations and ^{S}VIPAM analogs. PalmK-VIP-(KE)$_4$ (a), Palm$_2$K-VIP-(KE)$_4$ (b), Palm$_2$K-VIP-(KE)$_2$K$_4$ (c), and Palm$_2$K-VIP-(KE)$_2$E$_4$ (d) are shown in blue, whereas their scrambled counterparts (e–h) are shown in orange. All micrographs were taken at a magnification of 12 000× with the scale bar for all images set at 200 nm.

characterization results for all VIPA and ^{S}VIPA formulations are summarized in Table 2 to allow for easier comparisons among the data across different parameters. The micellization behavior of ^{S}VIPA formulations was relatively similar to that of VIPAs. The CMC of the single lipid ^{S}VIPA (*i.e.*, PalmK-^{S}VIP-(KE)$_4$, Fig. 4e – 2.85 μM) was found to be higher than its double lipid ^{S}VIPA analog (*i.e.*, Palm$_2$K-^{S}VIP-(KE)$_4$, Fig. 4f – 0.158 μM) which follows the same convention found for VIPAs. Additionally, two CMCs were observed for zwit-an double lipid ^{S}VIPA (*i.e.*, Palm$_2$K-^{S}VIP-(KE)$_2$E$_4$, Fig. 4h) similar to its corresponding VIP formulation (*i.e.*, Palm$_2$K-VIP-(KE)$_2$E$_4$, Fig. 4d). Interestingly, zwit double lipid ^{S}VIPA (*i.e.*, Palm$_2$K-^{S}VIP-(KE)$_4$, Fig. 4f) and zwit-cat double lipid ^{S}-VIPA (*i.e.*, Palm$_2$K-^{S}VIP-(KE)$_2$K$_4$, Fig. 4g) exhibited one and two CMCs, respectively, which is inverted from what was found for their analogous VIP formulations (*i.e.*, Fig. 4b – Palm$_2$K-VIP-(KE)$_4$ and Fig. 4c – Palm$_2$K-VIP-(KE)$_2$K$_4$).

Excitingly, all VIPA and ^{S}VIPA formulations formed micelles at the identified biological working concentration (*i.e.*, 5 μM), so the morphology of all VIPAMs and ^{S}VIPAMs at

this concentration was assessed using TEM (Fig. 5). To assist in describing nanoparticle shape, micelle architecture was divided into six categories: spheres ($L/D \sim 1$), short cylinders ($3 < L/D \leq 10$), small cylinders ($10 < L/D \leq 30$), medium cylinders ($30 < L/D \leq 100$), large cylinders ($100 < L/D \leq 300$), and long cylinders ($300 < L/D$). It was found that PalmK-VIP-(KE)$_4$ formed mostly large/long cylinders (1000–9000 nm in length), Palm$_2$K-VIP-(KE)$_4$ yielded almost exclusively small/medium cylinders (100–700 nm in length), Palm$_2$K-VIP-(KE)$_2$K$_4$ generated predominantly spheres (10–15 nm in length), and Palm$_2$K-VIP-(KE)$_2$E$_4$ created a mix of spheres (10–20 nm in diameter) and short/small cylinders (20–300 nm in length) (Fig. 5a–d). Single lipid VIPAs (*i.e.*, PalmK-VIP-(KE)$_4$) assembled into more elongated structures (Fig. 5a) compared to double lipid VIPAs (*i.e.*, Palm$_2$K-VIP-(KE)$_4$, Palm$_2$K-VIP-(KE)$_2$K$_4$, and Palm$_2$K-VIP-(KE)$_2$E$_4$) (Fig. 5b–d). The greater steric hindrance found in the hydrophobic core of double lipid VIPAMs in contrast to the single lipid VIPAMs likely resulted in much looser amphiphile packing causing the effective head group area (a_o) to be greater than the

Table 2 Structural characterization of VIPAs and ^{S}VIPAs

VIPAs	CMC (μM)	Zeta potential (mV)	Size (nm)	VIPAs	CMC (μM)	Zeta potential (mV)	Size (nm)
PalmK-VIP-(KE)$_4$ (mostly large/long cylinders)	0.333	−2.46 ± 6.96	—	PalmK-^{S}VIP-(KE)$_4$ (mostly large/long cylinders)	0.333	−0.774 ± 9.64	—
Palm$_2$K-VIP-(KE)$_4$ (small/medium cylinders)	0.0872 (1st) 0.409 (2nd)	12.5 ± 11.0	—	Palm$_2$K-^{S}VIP-(KE)$_4$ (spheres)	0.0872 (1st) 0.409 (2nd)	6.60 ± 10.2	41.0 ± 14.9
Palm$_2$K-VIP-(KE)$_2$K$_4$ (mostly spheres)	0.304	21.9 ± 12.6	55.8 ± 17.5	Palm$_2$K-^{S}VIP-(KE)$_2$K$_4$ (small/medium cylinders)	0.304	20.2 ± 14.6	—
Palm$_2$K-VIP-(KE)$_2$E$_4$ (spheres + short/small cylinders)	0.182 (1st) 2.72 (2nd)	−12.4 ± 5.44	—	Palm$_2$K-^{S}VIP-(KE)$_2$E$_4$ (spheres + short/small cylinders)	0.182 (1st) 2.72 (2nd)	12.6 ± 12.0	—

This journal is © The Royal Society of Chemistry and IChemE 2025
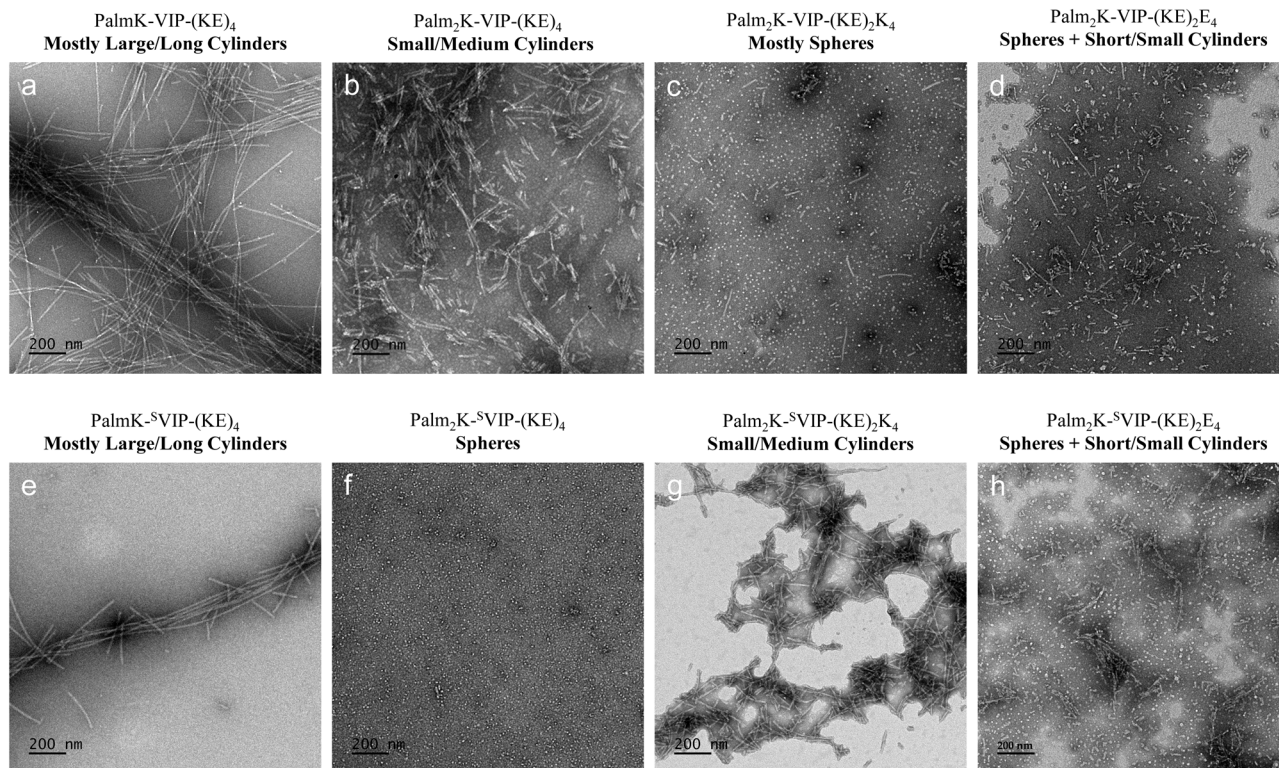
Fig. 5 Micelle morphologies of VIPAMs and ^{S}VIPAMs. PalmK-^{S}VIP-(KE)$_4$ (a), Palm$_2$K-^{S}VIP-(KE)$_4$ (b), Palm$_2$K-^{S}VIP-(KE)$_2$K$_4$ (c) and Palm$_2$K-^{S}VIP-(KE)$_2$E$_4$ (d), as well as their scrambled counterparts (e–h) were imaged with negative stain TEM. All micrographs were taken at a magnification of 12 000× with the scale bar for all images representing 200 nm.

doubling of the hydrocarbon core volume (v) leading to overall lower CPP values. This observation is similar to previously published results on the influence lipid number has on micelle size.[11] Furthermore, zwit-cat double lipid VIPA (*i.e.*, Palm$_2$K-VIP-(KE)$_2$K$_4$) and zwit-an double lipid VIPA (*i.e.*, Palm$_2$K-VIP-(KE)$_2$E$_4$) assembled into more compact micelles (*i.e.*, Fig. 5c and d – at least some population of spheres was found with both formulations) than zwit double lipid VIPA (*i.e.*, Fig. 5b – Palm$_2$K-VIP-(KE)$_4$ – only cylindrical micelles). This result suggested that corona-based charge repulsion was likely able to further increase effective head group area (a_o) leading to even greater micelle curvature. For ^{S}VIPAMs, the similarities and differences detected in the CMC profiles between VIPAs and ^{S}VIPAs with the same N-terminal and C-terminal chemical modifications was also reflected in their micellar morphologies. TEM images of PalmK-^{S}VIP-(KE)$_4$, Palm$_2$K-^{S}VIP-(KE)$_4$, Palm$_2$K-^{S}VIP-(KE)$_2$K$_4$, and Palm$_2$K-^{S}VIP-(KE)$_2$E$_4$ revealed their structures to be mostly large/long cylinders (1000–9000 nm in length), spheres (10–15 nm in diameter), small/medium cylinders (100–400 nm in length), and a mix of spheres (10–20 nm in diameter) and short/small cylinders (50–250 nm in length), respectively (Fig. 5e–h). Single lipid ^{S}VIPA (*i.e.*, Fig. 5e – PalmK-^{S}VIP-(KE)$_4$) and zwit-an double lipid ^{S}VIPA (*i.e.*, Fig. 5h – Palm$_2$K-^{S}VIP-(KE)$_2$E$_4$) possessed similar architectures as their VIPA counterparts (Fig. 5a and d). Remarkably, the other two ^{S}VIPA formulations flipped micelle shapes with their VIPA counterparts with compact micelles generated by zwit-cat double lipid ^{S}VIPA (Fig. 5g) and zwit double lipid VIPA (Fig. 5f) whereas mostly spherical micelles were present with zwit double lipid ^{S}VIPA (Fig. 5f) and zwit-cat double lipid VIPA (Fig. 5g). This inversion mimicked what was observed with CMCs further supporting the semi-stable spherical micelle shape found with some formulations.

After determining approximate micelle sizes using TEM, dynamic light scattering (DLS) was further employed to assess the size of spherical micelles in solution. PAM formulations which generated any elongated micelles were not measured due to limitations associated with this technique when used with moderate to high aspect ratio particles. Unsurprisingly, the diameters of spherical PAMs in solution ranged between 40–60 nm, approximately four times their dehydrated size, due to swelling of the hydrophilic PAM corona. In addition to size, surface charge was determined for each formulation as charge is known to play an important role in the toxicity and bioactivity of nanoparticles *in vivo*.[11] While differences were observed and are discussed below, it should be noted that all values are in a range of −25–+25 mV, which has typically not been extreme enough in either direction to greatly influence cell–nanoparticle interactions.[11,31–33] Balanced zwitterion-like PAs containing a single lipid tail were slightly negatively charged and overall more neutral than the double-lipid versions, which, given that both PAs contain the same quantity and composition of charged residues, may have stemmed from

structural differences and possible charge-shielding effects seen with nanoparticles possessing unique architectures.[34] Both zwit-cat PA formulations (*i.e.*, Palm$_2$K-VIP-(KE)$_2$K$_4$ and Palm$_2$K-^{S}VIP-(KE)$_2$K$_4$) were expectedly more positively charged, but interestingly therapeutic and scrambled zwit-an formulations diverged from one another. Specifically, Palm$_2$K-VIP-(KE)$_2$E$_4$ had a negative zeta potential whereas the scrambled analog (*i.e.*, Palm$_2$K-^{S}VIP-(KE)$_2$E$_4$) possessed an equivalent but positive charge. Although both of these formulations yield a mixture of spherical and short cylindrical micelles and contain the same composition of amino acids, it may be possible that differences in secondary structure within each PA play a crucial role in their folding given that the therapeutic and scrambled peptides are distinct in their specific sequence. Because peptide secondary structure has been demonstrated to play a profound role in influencing amphiphile packing and thus micelle size and shape,[35,36] such structure likely impacts the amino acid composition present on the micellar surface yielding different measured surface charge. Circular dichroism (CD) assessment of VIPAMs and ^{S}VIPAMs revealed exciting secondary structure differences between the formulations (Table 3). VIP and ^{S}VIP were found to contain a near even mix of organized secondary structure (*i.e.*, combined α-helix and β-sheet content – 49.4% and 46.6%, respectively) and disorganized secondary structure (*i.e.*, random coil content – 50.6% and 53.4%, respectively). In contrast to free peptides in solution, all VIPAM and ^{S}VIPAM formulations possessed considerably greater organized secondary structure content (*i.e.*, 65.7–100%) likely due to micellization itself. Confinement of PAs within micelles mimics an artificial tertiary structure which can induce and stabilize organized peptide secondary structure.[37] For single lipid micelles (*i.e.*, PalmK-VIP-(KE)$_4$ and PalmK-^{S}VIP-(KE)$_4$), considerable changes in the distribution of α-helical, β-sheet, and random coil content did little to impact their elongated cylindrical shape. In contrast, double lipid micelles displayed a clear relationship between shape and peptide secondary structure. Double lipid, spherical micelles (*i.e.*, Palm$_2$K-VIP-(KE)$_2$K$_4$ and Palm$_2$K-^{S}VIP-(KE)$_4$) possessed the greatest combined α-helix and random coil content (*i.e.*, 46.5% and 41.5%, respectively), while double lipid formulations with considerable cylindrical micelle populations (*i.e.*, Palm$_2$K-VIP-(KE)$_4$, Palm$_2$K-VIP-(KE)$_2$E$_4$, Palm$_2$K-^{S}VIP-(KE)$_2$K$_4$, and PalmK-^{S}VIP-(KE)$_2$E$_4$) contained a much lower quantity of these (*i.e.*, 0–13.3%). The bulky nature of α-helical and

random coil peptide secondary structures has been shown to promote spherical micelle formation, whereas β-sheet structures associated with tighter amphiphile packing and reduced a_o values driving cylindrical micelle production.[36] After examining the unique structural relationships between VIPAM and ^{S}VIPAM formulations, micelle–cell interactions mediated by VIP/VPAC binding were studied.

Cell association and uptake of micelles with varying chemical and physical properties

To investigate the influence VIPAMs and ^{S}VIPAMs with different shapes and sizes have on Mφs, initial (*i.e.*, 1 hour) and prolonged (*i.e.*, 6 hours) micelle/cell co-incubation was observed using confocal microscopy (Fig. 6 and 7). Green dot clusters located between the cell nucleus (blue) and cell membrane (red) were indicative of micelle internalization and denoted with yellow arrows. In contrast, yellow-green dot masses found co-localized with the cell membrane were considered surface-associated and highlighted with grey arrows. At the earlier time point, VIPAM chemistries capable of forming spherical micelles (*i.e.*, Palm$_2$K-VIP-(KE)$_2$K$_4$ and Palm$_2$-K-VIP-(KE)$_2$E$_4$) were found to be both associated with the cell surface of Mφs as well as between the membrane and nucleus (Fig. 6c and d). Conversely, VIPAMs which formed cylindrical micelles (*i.e.*, Palm$_2$K-VIP-(KE)$_4$ and PalmK-VIP-(KE)$_4$) were only found along the Mφ cell membrane (Fig. 6a and b). At 6 hours, Mφ-internalized micelles were found for all VIPAM chemistries that generated spherical and more compact cylindrical micelles (Fig. 6f–h) whereas the elongated cylindrical micelles made by PalmK-VIP-(KE)$_4$ remained solely associated with the cell surface (Fig. 6e). Mφ uptake of ^{S}VIPAM formulations that formed spherical and more compact cylindrical micelles (*i.e.*, Palm$_2$K-^{S}VIP-(KE)$_4$, Palm$_2$K-^{S}VIP-(KE)$_2$E$_4$, and Palm$_2$K-^{S}VIP-(KE)$_2$K$_4$) was observed at both time points (Fig. 7b–d and f–h). In contrast, limited Mφ association with and no internalization of elongated cylindrical PalmK-^{S}VIP-(KE)$_4$ micelles was observed throughout the experiment (Fig. 7a and e). The rapid internalization of spherical and short cylindrical micelles independent of peptide chemistry (Fig. 6c and d and 7c and d) aligns with effects expected from endocytosis of extracellular material under 100 nm in size.[38] Specifically, multiple endocytic pathways capable of internalizing extracellular material within this size range lead to no advantage of VPAC

Table 3 Secondary structure of VIPAMs and ^{S}VIPAMs

VIPAs	α-Helix	β-Sheet	Random Coil	^{S}VIPAs	α-Helix	β-Sheet	Random Coil
VIP	8.1%	41.3%	50.6%	^{S}VIP	7.9%	38.6%	53.4%
PalmK-VIP-(KE)$_4$ mostly large/long cylinders	18.9%	81.1%	0.0%	PalmK-^{S}VIP-(KE)$_4$ mostly large/long cylinders	33.7%	32.0%	34.3%
Palm$_2$K-VIP-(KE)$_4$ small/medium cylinders	13.3%	86.7%	0.0%	Palm$_2$K-^{S}VIP-(KE)$_4$ spheres	19.7%	58.5%	21.8%
Palm$_2$K-VIP-(KE)$_2$K$_4$ mostly spheres	17.3%	53.8%	28.9%	Palm$_2$K-^{S}VIP-(KE)$_2$K$_4$ small/medium cylinders	0.0%	100.0%	0.0%
Palm$_2$K-VIP-(KE)$_2$E$_4$ spheres + short/small cylinders	12.1%	87.9%	0.0%	Palm$_2$K-^{S}VIP-(KE)$_2$E$_4$ spheres + short/small cylinders	0.0%	100.0%	0.0%

542 | *Mol. Syst. Des. Eng.*, 2025, **10**, 534–548

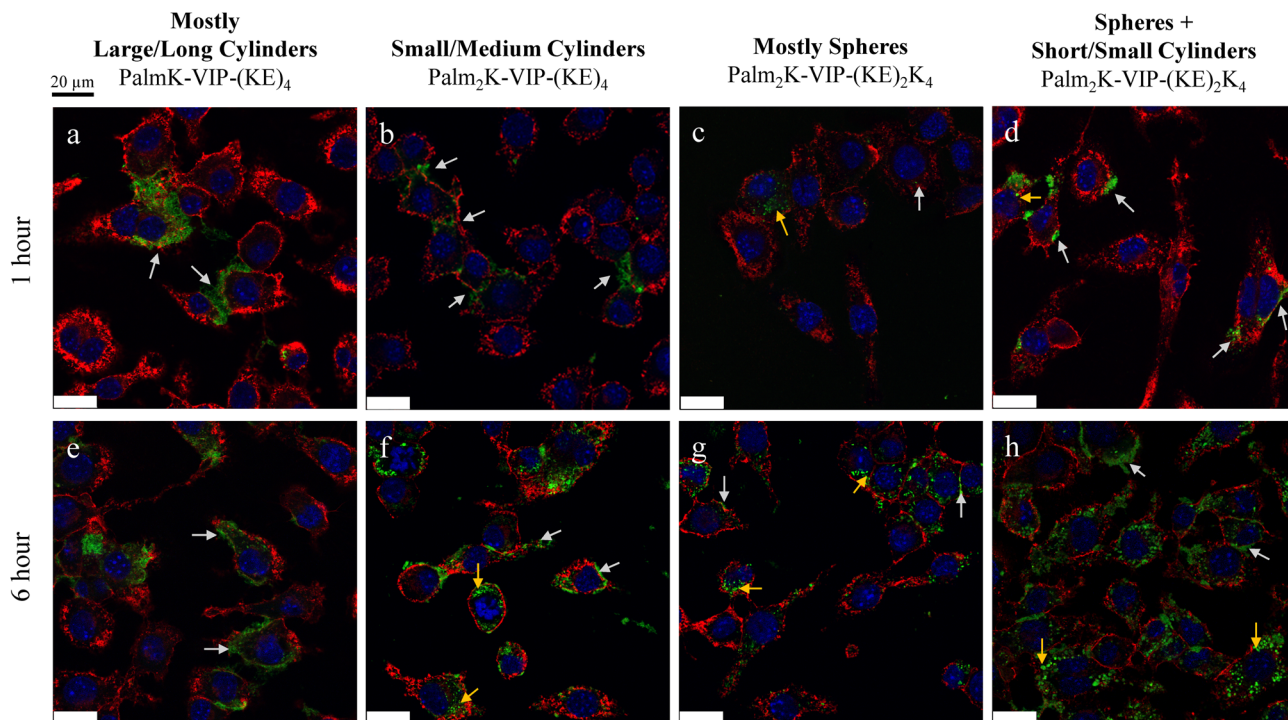This journal is © The Royal Society of Chemistry and IChemE 2025

Fig. 6 Representative confocal micrographs from 4 independent replicates of VIPAM association with Mφs at 1 hour (a–d) and 6 hours (e–h). The cell membrane and cell nucleus were stained by WGA (red) and DAPI (blue), respectively, whereas the FAM-labeled micelles appear in green. Yellow arrows indicate internalized micelles and grey arrows indicate micelles associated with the cell surface. Images were taken using a 40× lens for which the scale bar is equal to 20 μm.
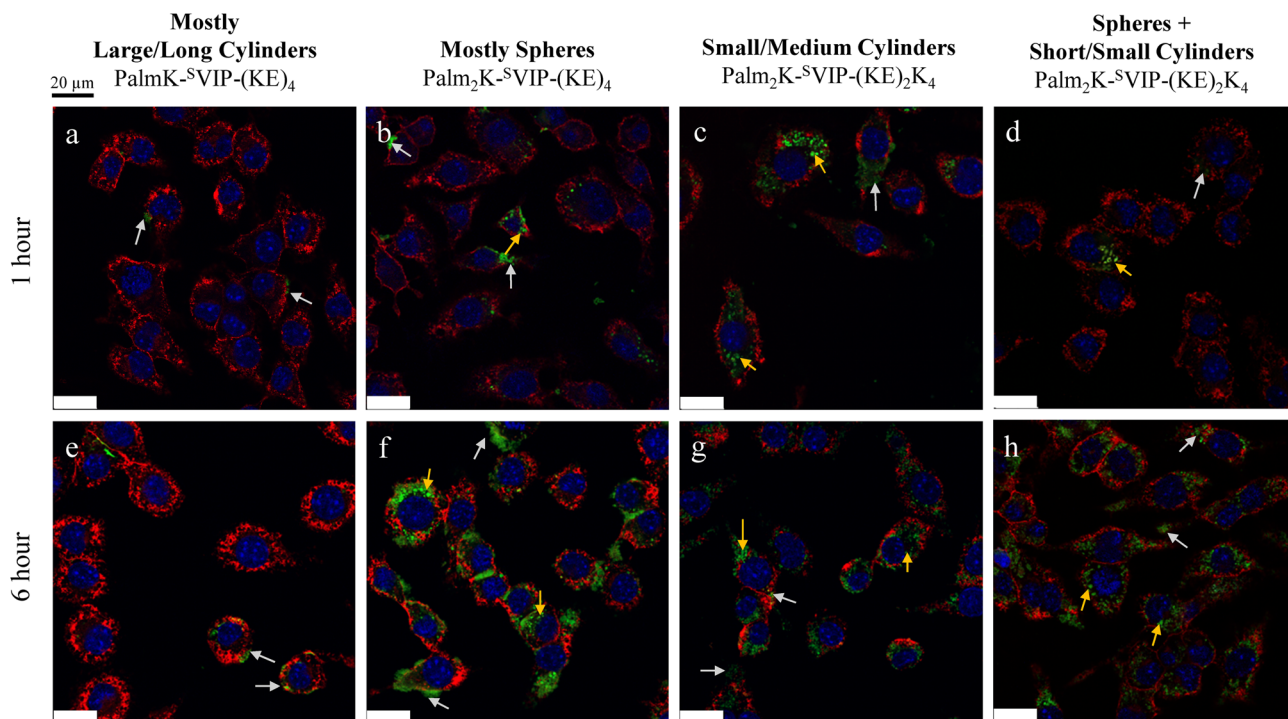

Fig. 7 Representative confocal micrographs from 4 independent replicates of ^{S}VIPAM association with Mφs at 1 hour (a–d) and 6 hours (e–h). The cell membrane and cell nucleus were stained by WGA (red) and DAPI (blue), respectively, whereas the FAM-labeled micelles appear in green. Yellow arrows indicate internalized micelles and grey arrows indicate micelles associated with the cell surface. Images were taken using a 40× lens for which the scale bar is equal to 20 μm.

targeting by VIPAMs over ^{S}VIPAMs. Interestingly, small/medium cylindrical micelle-inducing formulations possessed chemistry-dependent internalization speed with VIPAMs being uptaken by Mφs more slowly than ^{S}VIPAMs (Fig. 6b and f and 7c and g). Previous research has shown that intermediate-sized particles (*i.e.*, 300–3000 nm) are capable of fitting into the ruffles of the APC cell membrane more easily than their smaller or larger counterparts[12,19,39,40] and can be readily internalized by phagocytosis.[13,40] While ^{S}VIPAMs would be able to follow this relatively quick uptake pathway, VIPAMs likely bind their cognate surface receptor (*i.e.*, VPAC) localizing them there for longer periods of time. Previous research has found that Mφs can internalize materials by phagocytosis within an hour,[41] whereas significant VPAC internalization due to VIP binding[42] may take longer[43–45] and be inefficient for the internalization of intermediate-sized particles.[46] The chemistry-dependent association of long cylindrical micelles (>3000 nm) is unsurprising as these would be too large to fit into the cell membrane ruffles, so only those that could directly bind the cell surface (*i.e.*, VIPAMs to VPAC) would be capable of co-localizing with cells (Fig. 6a and e). Conversely, those that could not bind VPAC (*i.e.*, ^{S}VIPAMs) would be unable to facilitate prolonged contact with cells (Fig. 7a and e). The lack of internalization by surface-associated long cylindrical VIPAMs is expected as their size would require considerable cell membrane movement and reorganization which is a time- and energy-consuming process.[13] To better quantify the interesting effects that micelle shape and size have on cell association, the interactions VIPAMs and ^{S}VIPAMs have with co-incubated Mφs were also analyzed by flow cytometry.

Mφs were co-cultured with all micelle formulations for one and six hours, and the percentage of Mφs associated with fluorophore-labeled micelles as well as their median fluorescence intensity (MFI) were measured (Fig. 8 and 9). Unsurprisingly, micelle peptide specificity was found to play a crucial role in facilitating rapid cell association as Mφs were 2–10 times more likely to be associated with VIPAMs than their analogous ^{S}VIPAMs at the early time point (Fig. 8a). In addition, all tested VIPAMs, though possessing different morphologies, facilitated initial association with a similar percentage of Mφs suggesting this phenomenon was mainly regulated by cell surface receptor specificity regardless of micelle shape and size. Without this receptor-mediated effect, Mφs preferred to associate with small/medium cylindrical ^{S}VIPAMs (*i.e.*, Palm$_2$K-^{S}VIP-(KE)$_2$K$_4$) which can be efficiently entrapped in Mφ membrane ruffles. The MFI of fluorophore-labeled micelle-associated Mφs was relatively low for all formulations after 1 hour of co-incubation suggesting only a few micelles were associated with Mφs at this early time point (Fig. 8b). Large/long cylindrical VIPAMs displayed a slightly higher MFI relative to all other formulations resulting from their increased fluorescence signal per micelle.

At 6 hours, almost all Mφs were associated with co-cultured micelles regardless of their chemistry, shape, or size, besides large/long cylindrical ^{S}VIPAMs (*i.e.*, PalmK-^{S}VIP-(KE)$_4$) (Fig. 9a). Nearly 75% of Mφs were found associated
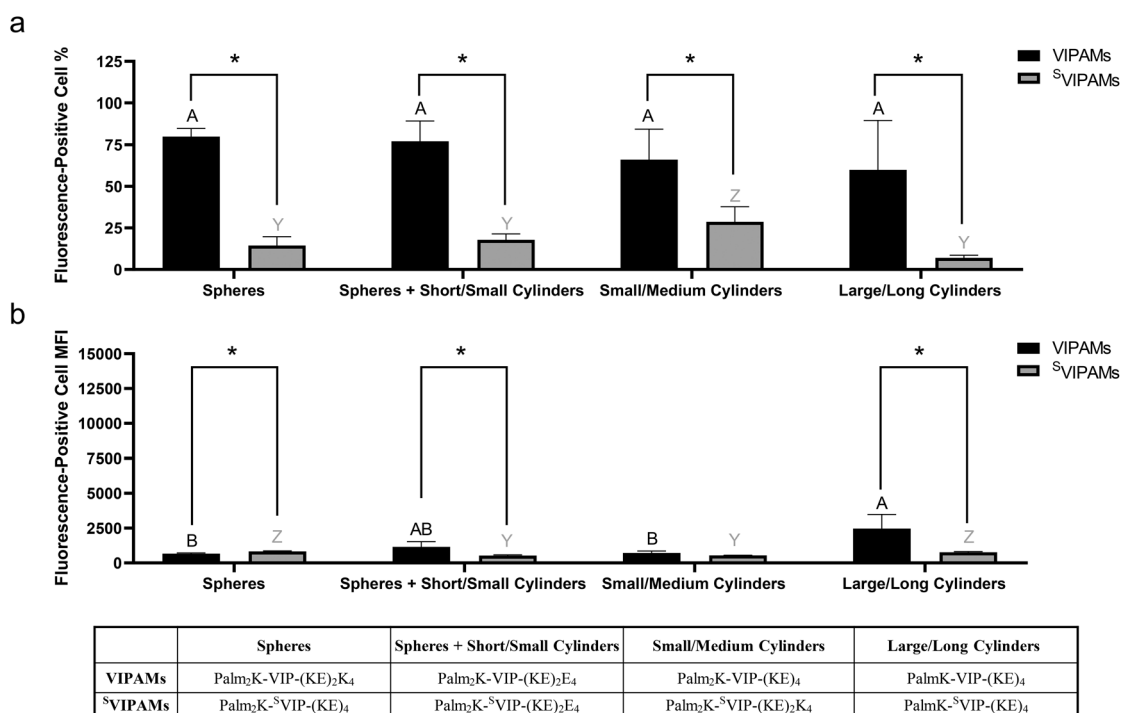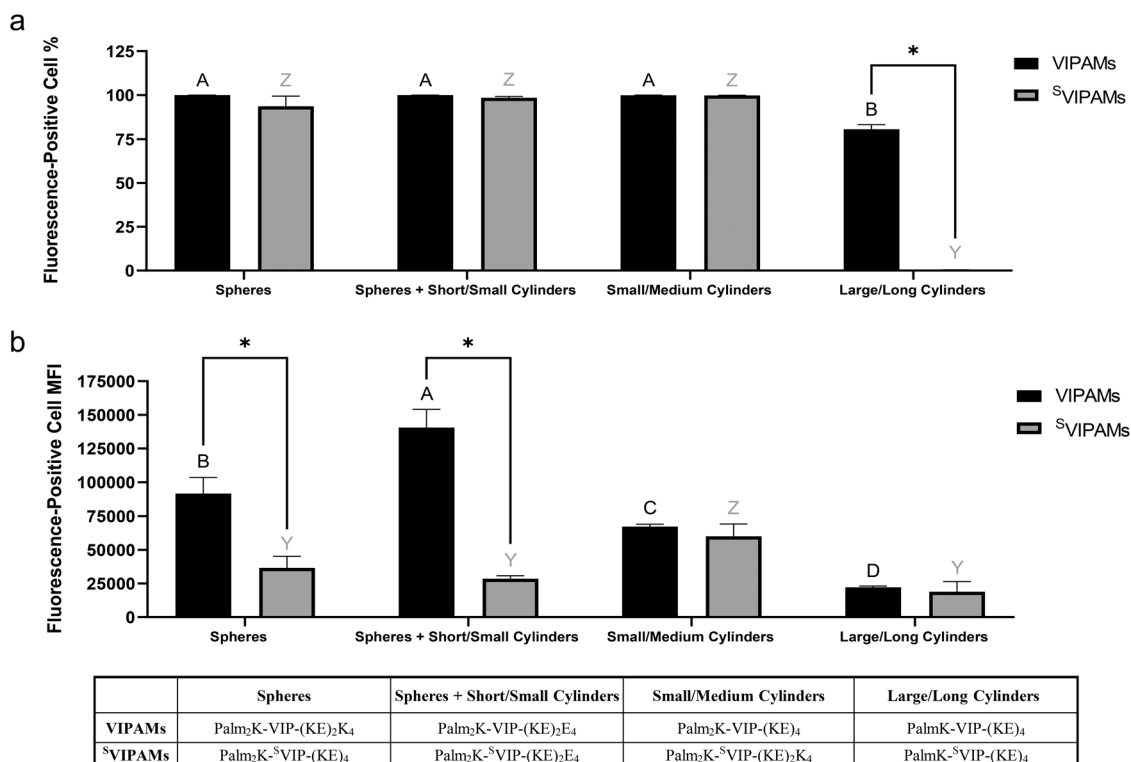

Fig. 8 Fluorescence-positive cell population to total cell population percentage (a) and mean fluorescence intensity (MFI) (b) of Mφs incubated for 1 hour with different shape and size VIPAMs or ^{S}VIPAMs ($n = 4$). In each graph, groups possessing the same letter or not possessing a star between them have no statistically significant difference ($p > 0.05$). Black (A–B) and grey (Y–Z) letters were used respectively to compare different shape and size VIPAMs or ^{S}VIPAMs, while * was used to compare VIPAMs and ^{S}VIPAMs that possessed the same shape and size.

	Spheres	Spheres + Short/Small Cylinders	Small/Medium Cylinders	Large/Long Cylinders
VIPAMs	Palm$_2$K-VIP-(KE)$_2$K$_4$	Palm$_2$K-VIP-(KE)$_2$E$_4$	Palm$_2$K-VIP-(KE)$_4$	PalmK-VIP-(KE)$_4$
^{S}VIPAMs	Palm$_2$K-^{S}VIP-(KE)$_4$	Palm$_2$K-^{S}VIP-(KE)$_2$E$_4$	Palm$_2$K-^{S}VIP-(KE)$_2$K$_4$	PalmK-^{S}VIP-(KE)$_4$

544 | *Mol. Syst. Des. Eng.*, 2025, **10**, 534–548

This journal is © The Royal Society of Chemistry and IChemE 2025

Fig. 9   Fluorescence-positive cell population to total cell population percentage (a) and mean fluorescence intensity (MFI) (b) of Mφs incubated for 6 hours with different shape and size VIPAMs or ^SVIPAMs ($n = 4$). In each graph, groups possessing the same letter or not possessing a star between them have no statistically significant difference ($p > 0.05$). Black (A–B) and grey (Y– Z) letters were used respectively to compare different shape and size VIPAMs or ^SVIPAMs, while * was used to compare VIPAMs and ^SVIPAMs that possessed the same shape and size.

with long cylindrical VIPAMs, but their low MFI suggests low numbers of micelles were present per cell with each micelle contributing a large fluorescent output. The large size and non-specificity of long cylindrical ^SVIPAMs greatly limited their association with Mφs and engulfment by Mφ membrane ruffles[13,19] as well, which aligns with prior data (Fig. 7e). The quantity of micelle association with Mφs, as reported by MFI, showed that VIPAM formulations that generate solely spherical (*i.e.*, P$_2$K-VIP-(KE)$_2$K$_4$) or solely small/medium cylindrical micelles (*i.e.*, Palm$_2$K-VIP-(KE)$_4$) had significantly higher MFIs compared with long cylinders, coinciding with their smaller size and improved ability to associate with and cross the cell membrane (Fig. 9b). Furthermore, spherical micelles displayed an even greater MFI over small/medium cylindrical micelles. Although less is known about the size of VPAC receptors, typical GPCr transmembrane segments have diameters capable of accommodating only very small micelles.[47] Because spherical micelles are made of less individual PAs, a greater number of total micelles would be formed upon reconstitution. Spherical micelles might then maximize VPAC receptor occupation relative to other VIPAM formulations as more micelles capable of interacting with their cognate receptors would be expected at any single time point. Interestingly, the greatest Mφ association was found with Palm$_2$K-VIP-(KE)$_2$E$_4$ which forms a mix of spherical and short/small cylindrical micelles, potentially reflecting the impact of PAM

size on Mφ association as well as the importance of fluorophore-labelled PA content per micelle. In contrast to spherical micelles, the largest-sized VIPAMs (*i.e.*, Palm$_2$K-VIP-(KE)$_4$ and PalmK-VIP-(KE)$_4$) contain much more PAs per micelle and thus possess more fluorophore-labelled PAs per micelle (~15–1500) as well, compared to the ~2–4 expected for spherical micelles. Association events between these bigger VIPAMs and VPAC receptor(s), though less in frequency, would yield a much higher fluorescence payload, though large micelle size might reduce Mφ VPAC occupancy due to shielding of unbound receptors. Palm$_2$K-VIP-(KE)$_2$E$_4$ forms both spherical and small cylindrical micelles, which may function synergistically to increase the number of receptor binding events and total delivered fluorescence payload. The sizeable spherical PAM population can accommodate many cell surface receptors, while the cylinders observed in this formulation may possess a somewhat high fluorophore per micelle content (~3–50), enhancing the resulting fluorescence signal. Moreover, their smaller size might circumvent the problem of shielding unbound receptors leading to efficient VPAC binding. This data corresponds well to the confocal microscopy results which showed co-incubated Mφs had their cell membranes coated by Palm$_2$K-VIP-(KE)$_2$E$_4$ micelles (Fig. 6h) to a much greater extent than all other VIPAM formulations (Fig. 6e–g).

Without cell surface receptor specificity, the MFI of Mφs associated with ^SVIPAMs remained lower than or similar to that

of Mφs contacting VIPAMs. All ^{S}VIPAM formulations except one demonstrated insignificantly different levels of cell interactions, with small/medium cylindrical ^{S}VIPAMs displaying an enhanced level of fluorescence similar to that of the structurally analogous VIPAMs. The relatively high uptake of nonspecific small/medium cylinders aligns with previous observations (Fig. 7f). With this formulation, VPAC specificity may slow down PA and PAM internalization over nonspecific micelles by localizing VIPAMs at their cognate receptors[43–45] preventing efficient cellular entry by phagocytosis. Comparing cell association across micelles with different peptide chemistry showed that all VIPAMs yielded greater or similar MFI values relative to their ^{S}VIPAM counterparts indicating the overall value of VPAC-based Mφ targeting.

Conclusion

This research provides significant insight into how modifications in lipid content and peptide sequence can be leveraged to generate PAMs of varying shapes and sizes which directly influences their association to and uptake by Mφs. Micelle morphology was greatly influenced by lipid tail steric hindrance as well as more finely manipulatable by minor changes in hydrophilic peptide block amino acid content. Interestingly, altering the position of the amino acids within the bioactive peptide region (i.e., using ^{S}VIP compared to VIP) modulated which double lipid PAs formed various nanostructures though batches of similar micelle architectures were able to be made regardless of whether VIP or ^{S}VIP was incorporated. Co-incubation of these various micelle formulations with Mφs revealed that presentation of cell targeting VIP over its scrambled peptide analog (i.e., ^{S}VIP) dictated rapid association with VIP, more so than micelle shape and size. That being said, prolonged micelle association with and internalization by Mφs was likely influenced by a combination of biomolecular material structure and chemistry as well as route of entry into cells. Although all VIPAMs demonstrated greater or similar levels of cellular association compared to ^{S}VIPAMs, structurally dissimilar micelles interacted with cells at different rates indicating potential differences in internalization mechanism. Smaller VPAC-specific micelles present in larger numbers may bind a large quantity of VPAC receptors while also exploiting other mechanisms of nonspecific internalization.[42–45] By contrast, slightly larger small/medium cylindrical micelles not specific to VPAC may actually benefit from non-specificity as these are more rapidly internalized by phagocytosis than VPAC-specific, smaller or larger particles.[12,13,19,38–40] From these studies, Palm$_2$K-VIP-(KE)$_2$E$_4$ was found to produce a mix of spherical and short/small cylindrical micelles from 10–300 nm in their largest dimension, which achieved the best Mφ association being able to be both internalized by cells and persist on the cell surface. While exciting, the influence micelle receptor specificity and material properties have on their bioactivity still needs to be further studied to help generate more detailed chemistry-structure–function relationships for immunomodulatory materials as well as specifically down select the formulation best capable of inducing productive and sustained anti-inflammatory effects for future clinical applications. The next step in this research involves comprehensive cytokine profiling, including pro-inflammatory markers such as IL-1β, IL-6, and IFN-γ as well as anti-inflammatory cytokines like IL-10 and TGF-β. These data, combined with in vivo studies in relevant disease models, will offer strong support for validating the therapeutic potential of VIPAMs, advancing their application in immunomodulatory research.

Data availability

All data enclosed in this paper is stored on laboratory hard drives and backed-up with cloud storage. None of the data is currently available on any publicly available database due to its propriety nature, but can be shared with interested parties on an as needed basis.

Conflicts of interest

There are no conflicts to declare.

Acknowledgements

References

1 D. Afonso-Oramas, L. Santana-Cordón, A. Lemus-Mesa, S. Teixidó-Trujillo, A. E. Rodríguez-Rodríguez, I. Cruz-Muros, M. González-Gómez and P. Barroso-Chinea, Drastic Decline in Vasoactive Intestinal Peptide Expression in the Suprachiasmatic Nucleus in Obese Mice on a Long-Term High-Fat Diet, Brain Res. Bull., 2023, 202, 110756, DOI: 10.1016/j.brainresbull.2023.110756.

2 W. Kittikulsuth, D. Nakano, K. Kitada, T. Uyama, N. Ueda, E. Asano, K. Okano, Y. Matsuda and A. Nishiyama, Vasoactive Intestinal Peptide Blockade Suppresses Tumor Growth by Regulating Macrophage Polarization and Function in CT26 Tumor-Bearing Mice, Sci. Rep., 2023, 13(1), 927, DOI: 10.1038/s41598-023-28073-6.

3 X. Yan, Y. Zhang, H. Lang, Z. Huang, X. Chen, H. He, Q. Zhao and J. Wang, Research on the Mechanism of Prednisone in the Treatment of ITP via VIP/PACAP-Mediated Intestinal Immune Dysfunction, Eur. J. Med. Res., 2023, 28, 67, DOI: 10.1186/s40001-023-00987-x.

546 | Mol. Syst. Des. Eng., 2025, 10, 534–548

This journal is © The Royal Society of Chemistry and IChemE 2025

4   H.-L. Zhong, P.-Z. Li, D. Li, C.-X. Guan and Y. Zhou, The Role of Vasoactive Intestinal Peptide in Pulmonary Diseases, *Life Sci.*, 2023, **332**, 122121, DOI: **10.1016/j.lfs.2023.122121**.

5   M. S. Al Najar and A. M. Lipchik, THU262 Improvement Of Pharmacokinetic Properties Of Vasoactive Intestinal Peptide Through Backbone Modifications, *J. Endocr. Soc.*, 2023, **7**(Suppl 1), bvad114.698, DOI: **10.1210/jendso/bvad114.698**.

6   R. Menacho-Melgar, J. S. Decker, J. N. Hennigan and M. D. Lynch, A Review of Lipidation in the Development of Advanced Protein and Peptide Therapeutics, *J. Controlled Release*, 2019, **295**, 1–12, DOI: **10.1016/j.jconrel.2018.12.032**.

7   J. Lau, P. Bloch, L. Schäffer, I. Pettersson, J. Spetzler, J. Kofoed, K. Madsen, L. B. Knudsen, J. McGuire, D. B. Steensgaard, H. M. Strauss, D. X. Gram, S. M. Knudsen, F. S. Nielsen, P. Thygesen, S. Reedtz-Runge and T. Kruse, Discovery of the Once-Weekly Glucagon-Like Peptide-1 (GLP-1) Analogue Semaglutide, *J. Med. Chem.*, 2015, **58**(18), 7370–7380, DOI: **10.1021/acs.jmedchem.5b00726**.

8   A. Trent, R. Marullo, B. Lin, M. Black and M. Tirrell, Structural Properties of Soluble Peptide Amphiphile Micelles, *Soft Matter*, 2011, **7**(20), 9572–9582, DOI: **10.1039/C1SM05862B**.

9   D. T. Seroski and G. A. Hudalla, in *Biomedical Applications of Functionalized Nanomaterials*, Micro and Nano Technologies, ed. B. Sarmento and J. das Neves, Elsevier, 2018, ch. 19 – Self-Assembled Peptide and Protein Nanofibers for Biomedical Applications, pp. 569–598, DOI: **10.1016/B978-0-323-50878-0.00019-7**.

10 D. Missirlis, T. Teesalu, M. Black and M. Tirrell, The Non-Peptidic Part Determines the Internalization Mechanism and Intracellular Trafficking of Peptide Amphiphiles, *PLoS One*, 2013, **8**(1), e54611, DOI: **10.1371/journal.pone.0054611**.

11 R. Zhang, J. D. Smith, B. N. Allen, J. S. Kramer, M. Schauflinger and B. D. Ulery, Peptide Amphiphile Micelle Vaccine Size and Charge Influence the Host Antibody Response, *ACS Biomater. Sci. Eng.*, 2018, **4**(7), 2463–2472, DOI: **10.1021/acsbiomaterials.8b00511**.

12 N. Doshi and S. Mitragotri, Macrophages Recognize Size and Shape of Their Targets, *PLoS One*, 2010, **5**(4), e10051, DOI: **10.1371/journal.pone.0010051**.

13 J. A. Champion and S. Mitragotri, Role of Target Geometry in Phagocytosis, *Proc. Natl. Acad. Sci. U. S. A.*, 2006, **103**(13), 4930–4934, DOI: **10.1073/pnas.0600997103**.

14 L. Leclerc, W. Rima, D. Boudard, J. Pourchez, V. Forest, V. Bin, P. Mowat, P. Perriat, O. Tillement, P. Grosseau, D. Bernache-Assollant and M. Cottier, Size of Submicrometric and Nanometric Particles Affect Cellular Uptake and Biological Activity of Macrophages in Vitro, *Inhalation Toxicol.*, 2012, **24**(9), 580–588, DOI: **10.3109/08958378.2012.699984**.

15 K. Donaldson, X. Y. Li, S. Dogra, B. G. Miller and G. M. Brown, Asbestos-Stimulated Tumour Necrosis Factor Release from Alveolar Macrophages Depends on Fibre Length and Opsonization, *J. Pathol.*, 1992, **168**(2), 243–248, DOI: **10.1002/path.1711680214**.

16 G. Sharma, D. T. Valenta, Y. Altman, S. Harvey, H. Xie, S. Mitragotri and J. W. Smith, Polymer Particle Shape Independently Influences Binding and Internalization by Macrophages, *J. Control Release*, 2010, **147**(3), 408–412, DOI: **10.1016/j.jconrel.2010.07.116**.

17 L.-J. Ma, R. Niu, X. Wu, J. Wu, E. Zhou, X.-P. Xiao and J. Chen, Quantitative Evaluation of Cellular Internalization of Polymeric Nanoparticles within Laryngeal Cancer Cells and Immune Cells for Enhanced Drug Delivery, *Nanoscale Res. Lett.*, 2021, **16**(1), 40, DOI: **10.1186/s11671-021-03498-y**.

18 T. Kusaka, M. Nakayama, K. Nakamura, M. Ishimiya, E. Furusawa and K. Ogasawara, Effect of Silica Particle Size on Macrophage Inflammatory Responses, *PLoS One*, 2014, **9**(3), e92634, DOI: **10.1371/journal.pone.0092634**.

19 T. Petithory, L. Pieuchot, L. Josien, A. Ponche, K. Anselme and L. Vonna, Size-Dependent Internalization Efficiency of Macrophages from Adsorbed Nanoparticle-Based Monolayers, *Nanomaterials*, 2021, **11**(8), 1963, DOI: **10.3390/nano11081963**.

20 C.-Y. Tsai, S.-L. Lu, C.-W. Hu, C.-S. Yeh, G.-B. Lee and H.-Y. Lei, Size-Dependent Attenuation of TLR9 Signaling by Gold Nanoparticles in Macrophages, *J. Immunol.*, 2012, **188**(1), 68–76, DOI: **10.4049/jimmunol.1100344**.

21 X. Xie, J. Liao, X. Shao, Q. Li and Y. Lin, The Effect of Shape on Cellular Uptake of Gold Nanoparticles in the Forms of Stars, Rods, and Triangles, *Sci. Rep.*, 2017, **7**(1), 3827, DOI: **10.1038/s41598-017-04229-z**.

22 T. Stern, I. Kaner, N. Laser Zer, H. Shoval, D. Dror, Z. Manevitch, L. Chai, Y. Brill-Karniely and O. Benny, Rigidity of Polymer Micelles Affects Interactions with Tumor Cells, *J. Controlled Release*, 2017, **257**, 40–50, DOI: **10.1016/j.jconrel.2016.12.013**.

23 X. Wang, R. Zhang, B. D. Lindaman, C. N. Leeper, A. G. Schrum and B. D. Ulery, Vasoactive Intestinal Peptide Amphiphile Micelle Chemical Structure and Hydrophobic Domain Influence Immunomodulatory Potentiation, *ACS Appl. Bio Mater.*, 2022, **5**(4), 1464–1475, DOI: **10.1021/acsabm.1c00981**.

24 A. Makovitzki, J. Baram and Y. Shai, Antimicrobial Lipopolypeptides Composed of Palmitoyl Di- and Tricationic Peptides: In Vitro and in Vivo Activities, Self-Assembly to Nanostructures, and a Plausible Mode of Action, *Biochemistry*, 2008, **47**(40), 10630–10636, DOI: **10.1021/bi8011675**.

25 J. Israelachvili, *Intermolecular and Surface Forces*, 3rd edn, 2011.

26 Ö. Farkas, E. Lajkó, M. Kalabay and K. N. Enyedi, How to Scramble? A "Wise Way" to Achieve a Useful Control Peptide Sequence, *SSRN Electron. J.*, 2023, DOI: **10.2139/ssrn.4363258**.

27 P. Nicole, L. Lins, C. Rouyer-Fessard, C. Drouot, P. Fulcrand, A. Thomas, A. Couvineau, J. Martinez, R. Brasseur and M. Laburthe, Identification of Key Residues for Interaction of Vasoactive Intestinal Peptide with Human VPAC1 and VPAC2 Receptors and Development of a Highly Selective VPAC1 Receptor Agonist. Alanine Scanning and Molecular Modeling

This journal is © The Royal Society of Chemistry and IChemE 2025

Mol. Syst. Des. Eng., 2025, **10**, 534–548 | **547**

of the Peptide, *J. Biol. Chem.*, 2000, **275**(31), 24003–24012, DOI: **10.1074/jbc.M002325200**.

28 M. L. E. Lundahl, S. Fogli, P. E. Colavita and E. M. Scanlan, Aggregation of Protein Therapeutics Enhances Their Immunogenicity: Causes and Mitigation Strategies, *RSC Chem. Biol.*, 2021, **2**(4), 1004–1020, DOI: **10.1039/d1cb00067e**.

29 R. Ni, L. Jiang, C. Zhang, M. Liu, Y. Luo, Z. Hu, X. Mou and Y. Zhu, Biologic Mechanisms of Macrophage Phenotypes Responding to Infection and the Novel Therapies to Moderate Inflammation, *Int. J. Mol. Sci.*, 2023, **24**(9), 8358, DOI: **10.3390/ijms24098358**.

30 D. C. Poland and H. A. Scheraga, Hydrophobic Bonding and Micelle Stability; the Influence of Ionic Head Groups, *J. Colloid Interface Sci.*, 1966, **21**(3), 273–283, DOI: **10.1016/0095-8522(66)90012-2**.

31 L. Landgraf, I. Müller, P. Ernst, M. Schäfer, C. Rosman, I. Schick, O. Köhler, H. Oehring, V. V. Breus, T. Basché, C. Sönnichsen, W. Tremel and I. Hilger, Comparative Evaluation of the Impact on Endothelial Cells Induced by Different Nanoparticle Structures and Functionalization, *Beilstein J. Nanotechnol.*, 2015, **6**(1), 300–312, DOI: **10.3762/bjnano.6.28**.

32 D. Hühn, K. Kantner, C. Geidel, S. Brandholt, I. De Cock, S. J. H. Soenen, P. Rivera Gil, J.-M. Montenegro, K. Braeckmans, K. Müllen, G. U. Nienhaus, M. Klapper and W. J. Parak, Polymer-Coated Nanoparticles Interacting with Proteins and Cells: Focusing on the Sign of the Net Charge, *ACS Nano*, 2013, **7**(4), 3253–3263, DOI: **10.1021/nn3059295**.

33 R. Zhang, B. T. Rygelski, L. E. Kruse, J. D. Smith, X. Wang, B. N. Allen, J. S. Kramer, G. F. Seim, T. J. Faulkner, H. Kuang, E. Kokkoli, A. G. Schrum and B. D. Ulery, Adjuvant Delivery Method and Nanoparticle Charge Influence Peptide Amphiphile Micelle Vaccine Bioactivity, *BioRxiv*, Prepr. Serv. Biol., 2024, preprint, DOI: **10.1101/2024.06.10.598369**.

34 R. Zhang, L. D. Morton, J. D. Smith, F. Gallazzi, T. A. White and B. D. Ulery, Instructive Design of Triblock Peptide Amphiphiles for Structurally Complex Micelle Fabrication, *ACS Biomater. Sci. Eng.*, 2018, **4**(7), 2330–2339, DOI: **10.1021/acsbiomaterials.8b00300**.

35 R. E. Sallach, M. Wei, N. Biswas, V. P. Conticello, S. Lecommandoux, R. A. Dluhy and E. L. Chaikof, Micelle Density Regulated by a Reversible Switch of Protein Secondary Structure, *J. Am. Chem. Soc.*, 2006, **128**(36), 12014–12019, DOI: **10.1021/ja0638509**.

36 T. Shimada, S. Lee, F. S. Bates, A. Hotta and M. Tirrell, Wormlike Micelle Formation in Peptide-Lipid Conjugates Driven by Secondary Structure Transformation of the Headgroups, *J. Phys. Chem. B*, 2009, **113**(42), 13711–13714, DOI: **10.1021/jp901727q**.

37 R. Zhang, C. N. Leeper, X. Wang, T. A. White and B. D. Ulery, Immunomodulatory Vasoactive Intestinal Peptide Amphiphile Micelles, *Biomater. Sci.*, 2018, **6**(7), 1717–1722, DOI: **10.1039/c8bm00466h**.

38 L. Kou, J. Sun, Y. Zhai and Z. He, The Endocytosis and Intracellular Fate of Nanomedicines: Implication for Rational Design, *Asian J. Pharm. Sci.*, 2013, **8**(1), 1–10, DOI: **10.1016/j.ajps.2013.07.001**.

39 M. V. Baranov, M. Kumar, S. Sacanna, S. Thutupalli and G. van den Bogaart, Modulation of Immune Responses by Particle Size and Shape, *Front. Immunol.*, 2020, **11**, 607945, DOI: **10.3389/fimmu.2020.607945**.

40 J. A. Champion, A. Walker and S. Mitragotri, Role of Particle Size in Phagocytosis of Polymeric Microspheres, *Pharm. Res.*, 2008, **25**(8), 1815–1821, DOI: **10.1007/s11095-008-9562-y**.

41 R. M. Gilberti and D. A. Knecht, Macrophages Phagocytose Nonopsonized Silica Particles Using a Unique Microtubule-Dependent Pathway, *Mol. Biol. Cell*, 2015, **26**(3), 518–529, DOI: **10.1091/mbc.E14-08-1301**.

42 D. Schulz, Y. Severin, V. R. T. Zanotelli and B. Bodenmiller, In-Depth Characterization of Monocyte-Derived Macrophages Using a Mass Cytometry-Based Phagocytosis Assay, *Sci. Rep.*, 2019, **9**(1), 1925, DOI: **10.1038/s41598-018-38127-9**.

43 I. Langer, Mechanisms Involved in VPAC Receptors Activation and Regulation: Lessons from Pharmacological and Mutagenesis Studies, *Front. Endocrinol.*, 2012, **3**, 129, DOI: **10.3389/fendo.2012.00129**.

44 C. Langlet, N. Gaspard, I. Nachtergael, P. Robberecht and I. Langer, Comparative Efficacy of VIP and Analogs on Activation and Internalization of the Recombinant VPAC2 Receptor Expressed in CHO Cells, *Peptides*, 2004, **25**(12), 2079–2086, DOI: **10.1016/j.peptides.2004.08.017**.

45 I. Langer, C. Langlet and P. Robberecht, Effect of Inactivating Mutations on Phosphorylation and Internalization of the Human VPAC2 Receptor, *J. Mol. Endocrinol.*, 2005, **34**(2), 405–414, DOI: **10.1677/jme.1.01717**.

46 C. Langlet, I. Langer, P. Vertongen, N. Gaspard, J.-M. Vanderwinden and P. Robberecht, Contribution of the Carboxyl Terminus of the VPAC1 Receptor to Agonist-Induced Receptor Phosphorylation, Internalization, and Recycling, *J. Biol. Chem.*, 2005, **280**(30), 28034–28043, DOI: **10.1074/jbc.M500449200**.

47 E. Serebryany, G. A. Zhu and E. C. Y. Yan, Artificial Membrane-like Environments for in Vitro Studies of Purified G-Protein Coupled Receptors, *Biochim. Biophys. Acta, Biomembr.*, 2012, **1818**(2), 225–233, DOI: **10.1016/j.bbamem.2011.07.047**.

548 | *Mol. Syst. Des. Eng.*, 2025, **10**, 534–548

This journal is © The Royal Society of Chemistry and IChemE 2025